

Universal limit on spatial quantum superpositions with massive objects due to phonons

Carsten Henkel*

University of Potsdam, Institute of Physics and Astronomy, Germany

Ron Folman†

Department of Physics, Ben-Gurion University of the Negev, Beer Sheva, Israel

(Dated: 21 May 2023)

The superposition principle is one of the founding principles of quantum theory. Spatial quantum superpositions have so far been tested only with small systems, from photons [1] and elementary particles [2–5] to atoms [6–8] and molecules [9, 10]. Such superpositions for massive objects have been a long-standing sought-after goal [11–19]. This is important not only in order to confirm quantum theory in new regimes, but also in order to probe the quantum-gravity interface. In addition, such an experiment will enable to test exotic theories [20–24], and may even enable new technology [25]. Creating such superpositions is notoriously hard because of environmental decoherence [19, 22, 26–30], whereby the large object couples strongly to the environment which turns the delicate quantum state into a statistical mixture (classical state). However, advances in the technology of isolation could in future suppress such decoherence. Here we present a decoherence channel which is not external but internal to the object, and consequently improved isolation would not help. This channel originates from the phonons (sound waves) within the object. We show that such phonons are excited as part of any splitting process, and thus we establish a fundamental and universal limit on the possibility of future spatial quantum superpositions with massive objects.

I. INTRODUCTION

Quantum phenomena with massive objects such as entanglement [31, 32] and superposition [33, 34] have been experimentally realised. However, the long-sought-after massive-object superposition over a significant spatial extent, a goal of paramount importance, remains elusive. To create such a state, one needs to start with a single object and then apply a splitting force so that the object splits in real space into two exact copies mirroring the original object, but with opposite momentum components. According to standard quantum theory, these copies, which are named wavepackets, are not “elements of reality”. Namely, we should not consider them as existing unless measured, in which case, only one of the wavepackets will become an element of reality. However, quantum theory allows us to calculate the properties of these individual wavepackets as if they were real objects. This is crucial as it allows us to evaluate the contrast of an interference pattern that may be formed if the two wavepackets are eventually joined (thus closing a loop in space-time). Such an interference pattern is the only way to prove that indeed a coherent quantum superposition was formed. To give an example of the fundamental implications, we recall that because Stern and Gerlach (SG) did not combine the two beams in their seminal experiment to show an interference pattern [35], a century of debate ensued of whether SG splitting with macroscopic magnets can indeed create a spatial quantum superposition of atoms (see [18] and references therein). This

debate has only recently been experimentally put to rest [8, 18, 36].

In this letter we calculate the developed orthogonality for a spatial superposition of a massive object. In simple terms, orthogonality is a measure of how different the two wavepackets have become after the splitting. This is also sometimes referred to as “*welcher Weg* information” or simply loss of coherence. When there is strong orthogonality, no interference pattern is possible, and consequently, no proof can be obtained that a spatial superposition has been formed.

Standard estimations of orthogonality involve two channels, namely, the coupling to the environment (typically referred to as decoherence [37, 38]), or the imperfect closing of the interferometer loop (imprecise recombination) which has been coined the Humpty-Dumpty effect [39–41]. For minimal orthogonality in the latter process, a complete overlap (identity) of position, momentum, and even wavepacket size and shape, at the recombination point, is required. In the following, we assume the above two channels do not produce orthogonality, and we focus our attention only on the topic of this paper, by estimating the amount of orthogonality produced by degrees of freedom which are unique to massive objects, phonons.

Phonons are internal sound waves which amount to density or shear waves inside the bulk. They are excited once some of the atoms are moved relative to others. The above noted splitting force, which must be used in order to create a spatial superposition, acts on the atoms of the bulk, and the crucial question is, how homogeneously? If different atoms feel a slightly different force, phonons will be excited. Since, in order to achieve a splitting, the forces acting on the two wavepackets must be of opposite

* carsten.henkel@uni-potsdam.de

† folman@bgu.ac.il

sign (direction), the excited phonons must consequently have a different sign or phase, and this gives rise to orthogonality.

II. MAIN

Let us adopt a universal model for the splitting process, independent of a specific material or interaction. We consider a potential $\alpha_i U(x)$ which acts on the object, where U is some field intensity and α_i is the coupling to the specific material of the object, with index i specifying which atom in the lattice is considered. The force acting on a specific position in the object or on a specific atom is thus $F = -\alpha_i U'(x)$, where the derivative is evaluated at the position of the atom. We neglect higher-order effects such as how the material changes the external field (e.g., due to absorption and polarizability). To avoid phonons from being excited we require that the force is completely homogeneous over the extent of each wavepacket. This means first that $\delta U'$, describing how far from constant is the potential gradient across the extent of the object, should be very small, and second that $\delta\alpha$, describing how far from homogeneous is the coupling to the potential gradient, should be very small. Specifically, $\delta\alpha$ is a measure of to what degree the atoms in the material are all the same (i.e., how pure the material is), and to what degree their density and orientation is the same across the object (e.g., no geometrical defects). In more abstract terms, one must demand the ultimate translational invariance of the force F .

In [42] we calculated this effect for a specific splitting interaction, a Stern-Gerlach (SG) magnetic gradient field. Here we generalise this result to any interaction and any material by using as the figure of merit the fractional inhomogeneity of the force, $\delta F/F$. Like in the SG interferometer, one may assume a general closed-loop symmetric configuration in which four equal (up to a sign) forces are applied, each of duration $\frac{1}{4}\Delta t$, for splitting, stopping the relative motion, accelerating back, and again stopping the relative motion for a full overlap in position and momentum.

While $\delta F/F$ should be represented by a power spectrum, we are only interested in its intensity at spatial frequencies (k vectors) from the inverse of the atomic interspacing to the inverse of the object size. An example for a k vector at the extreme of the inverse of the atomic interspacing may be taken from an inhomogeneous material whereby spin contaminations giving rise to a Stern-Gerlach force are randomly scattered throughout the object (e.g., a single or many nitrogen-vacancy centres within the spinless ^{12}C lattice of a diamond) [18]. An example for a k vector at the extreme of the inverse of the object size may be taken from an inhomogeneous force causing a collective stretching of the object. Such an effect would originate from an inverse harmonic potential [43] or from tidal forces due to gravity. Let us briefly note that in principle, since for large objects one would

need to apply a force for long durations Δt to get a meaningful spatial splitting, the Fourier transform of such a long pulse results in low frequencies. Consequently, k vectors at the extreme of the inverse of the atomic interspacing will be relatively suppressed, as they require high frequencies. Specifically, if we take the velocity of sound in the bulk to be of the order of $c = 1000 \text{ m/s}$ and the inter-atomic spacing to be 10^{-10} m , the required frequencies are 10^{13} Hz . This “Debye frequency” would require pulse durations of the applied force shorter than pico-second and concomitant large accelerations, unrealistic for large-object splitting. For the same reason of not considering ultra-short Δt , we will be neglecting the optical phonon branch. Hence, in the following we will be calculating a lower bound on the produced orthogonality. In Fig. 1 we present the phonon modes we are taking into account [see Supplementary Information (SI) for more details].

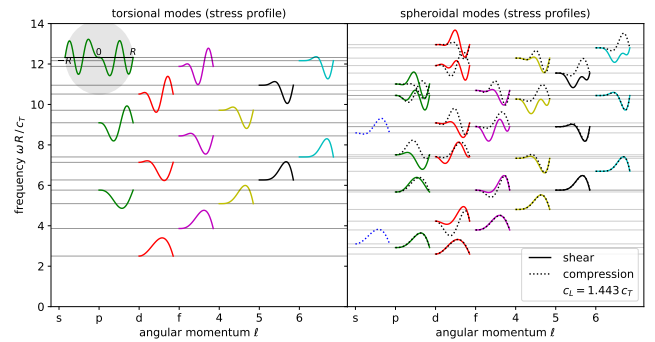


FIG. 1. Mode functions for elastic sound waves in a solid sphere, according to [44] and [45]. The ratio of the two speeds of sound is taken for silicon. For a sphere with diameter $2R = 1 \mu\text{m}$, the torsional d-waves (left) provide the fundamental tone at $\omega/2\pi \approx 2.501 c_T/(2\pi R) \approx 4.652 \text{ GHz}$, while spheroidal d-, p, and s-waves (right) are slightly higher in frequency. When multiplied with spherical harmonics or their derivatives, the plotted scalar functions represent the compressional and shear stress from 0 to R , and they vanish on the sphere surface. In the top left corner, one full mode is shown from $-R$ to R .

Let us emphasise that long Δt is not a simple experimental requirement to fulfil as it is well known that the larger the mass of an object the harder it is to isolate it from the environment and the faster the decoherence rate. But we assume that future technology will indeed enable near-perfect isolation. It turns out that long Δt also helps to minimise phonons. Specifically, in the following we show that adiabaticity, achieved with a slow and smooth rise of the splitting force, is beneficial for avoiding phonon excitation. In Fig. 2 we present three force profiles in time with varying degree of adiabaticity, and we will use these profiles to show the effect of force adiabaticity on phonon excitation and formation of orthogonality.

As an example of the formation of orthogonality, we present in Fig. 3 a phase-space diagram of the trajec-

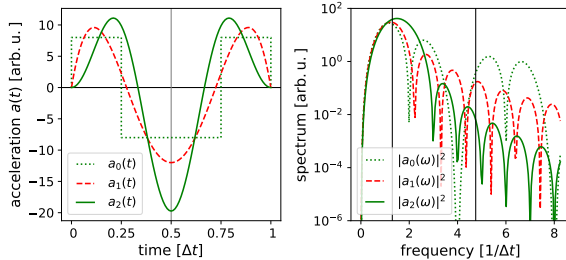


FIG. 2. Three different profiles for the splitting force [in time (left) and in frequency (right)], represented by $a_n(t)$, $n = 0, 1, 2$. They have in common the same maximum spatial splitting but differ in the degree of discontinuity as the force is switched on and off. The first corresponds to a rectangular profile (the force flips sign instantaneously at $t = \frac{1}{4}, \frac{3}{4}\Delta t$), so less adiabatic, while the other two are more adiabatic. (Left) As explained in the text, four force regions are included for splitting, stopping the relative motion, accelerating back, and again stopping the relative motion for a full overlap in position and momentum. (Right) A Fourier transform of the force profiles in time, where as expected, the rectangular profile gives rise to much higher (nonadiabatic) frequencies. The vertical lines mark the phonon frequencies considered in Fig. 3.

ries of phonon mode amplitudes in the two wavepackets. As can be seen, once separated, they never fully overlap again. While in Fig. 2 we present force profiles intended to close a loop in the standard phase-space of position and momentum, in Fig. 3 we address the unique phase-space of phonons. It is in this phase-space that the unclosed loops create the intrinsic orthogonality discussed in this work.

The details of our full calculation appear in the SI. Let us briefly summarise them: one computes from the forces on the atoms in the object the excitation of a given phonon mode. At the quantum level, this has the structure of a “displacement operator” creating a “coherent state”. The overlap after applying opposite displacements, evolving along the two arms from a thermal equilibrium state, is computed for each phonon mode. This gives rise to a formula resembling the Debye-Waller factor, where the internal phonon temperature and the size of the displacement appear. In the harmonic approximation, the total state of all phonon modes is a tensor product, and the total overlap a product of overlaps per mode. We take a statistical average of this product by assuming that the forces on the atoms have a simple correlation function, namely that their power spectrum is “spatially white noise” with a given amplitude $\delta F/F$. The result is the exponential of a sum over phonon modes where only the mode frequency and the mode degeneracy matters. For a solid sphere, Horace Lamb has computed back in 1881 the phonon modes, and the eigenfrequencies are related to zeros of the spherical Bessel functions. They depend only on the ratio c/D , namely the speed of sound over the diameter, so that a simple re-scaling gives the spectrum for a sphere of any size. One may

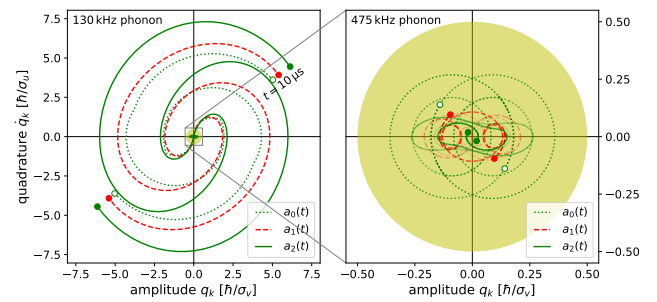


FIG. 3. Illustration of phonon orthogonality: the amplitude of a given phonon mode evolves under the applied splitting force pulse, proportional to the projection of the inhomogeneous force profile onto the spatial mode pattern [Supplementary Information, Eq.(4)]. The plots depict the trajectories in phase-space for forces with opposite signs, on the horizontal axis the mode’s excitation amplitude q_k , on the vertical the corresponding in-quadrature component $q_{\bar{k}}$. The parameters are taken for a pulse duration of $10\ \mu\text{s}$, a targeted maximum spatial splitting of $0.1\ \mu\text{m}$ (maximum acceleration of the order of $10^3\ \text{m/s}^2$), $\delta F/F = 1\%$, and a temperature $T = 4\ \text{K}$ (de Broglie wavelength of a single atom $\approx 0.1\ \text{nm}$). The quadratures $q_k, q_{\bar{k}}$ are made dimensionless by dividing by the corresponding coherence lengths in the initial thermal state [see Eq. (13)]. The yellow circle of unit diameter corresponds to the coherence area of the initial state: outside it, the contrast drops below $1/e$. (Left) Relatively low frequency: at the end of the applied force pulse, the phonon excitation is so large (dots) that the two interferometer arms can be distinguished on the scale of the coherence of the initial state (yellow circle). A single low-frequency mode in the object’s phonon spectrum would ruin the interference contrast. (Right) Higher frequency: during the applied pulse, the mode follows a more complex dynamics (the initial stage is faded out for better visualisation), but the final excitation is much weaker. To reduce the contrast significantly, many high-frequency modes must be excited. The line styles correspond to the acceleration protocols of Fig. 2 with increasing degree of adiabaticity. The chosen frequencies correspond to $\omega_k \Delta t/2\pi = 1.3, 4.75$, i.e., the vertical lines in Fig. 2 (right).

say that an object is “small” when a discrete summation over mode frequencies needs to be done. It is “large” when this sum is well approximated by an integral. The resulting contrast is universal, as it only depends on the object volume, independent of its shape, and of course, as noted, it is not dependent on any specific potential.

The final results are presented in Fig. 4, where we compare the decoherence due to phonons to that due to black-body radiation (BBR, see SI, Sec. S4), as a function of the spatial splitting and the object size. We consider $\delta F/F = 1\%$, different object temperatures and materials, as well as different force-adiabaticity profiles. When the interference experiment is performed in perfect vacuum, BBR is considered the dominant process for environmental decoherence [37, 46]. In the shaded areas above or to the right of the lines, the interference contrast drops below $1/e$ and rapidly becomes negligible. We allow for a

maximal acceleration of $10g$ (g being the gravitational acceleration on Earth), which seems reasonable for large objects. For lower accelerations, splitting and recombining takes a longer time, and isolation becomes even more of a challenge. Nevertheless, for completeness, we provide plots for maximum accelerations of $0.1g$ and the $1g$ plots in the SI, Fig. S1.

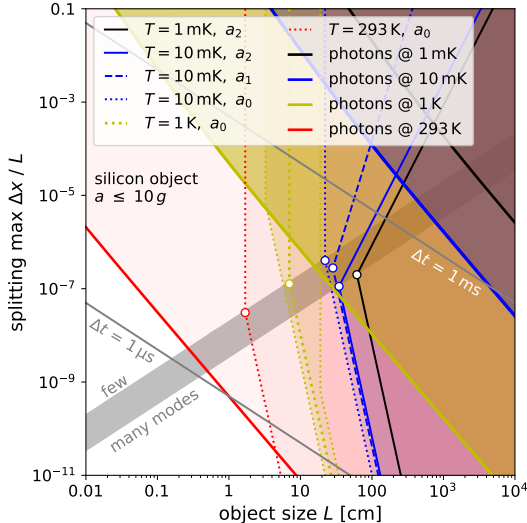


FIG. 4. Parameter space of decoherence. Shown are lines of phonon- or photon-induced contrast reduction to $1/e$: in the shaded areas, the contrast rapidly becomes negligible. Thick colored lines: decoherence due to photon absorption or emission from a blackbody spectrum with temperatures $T = 293\text{ K}$ (red), 1 K (yellow), 10 mK (blue), and 1 mK (black), computed from the momentum diffusion constant quoted in [22, 26] (see also [46]). Dotted (dashed, solid) lines with kinks: decoherence due to phonon excitation by a spherical object at the same temperatures, assuming a force heterogeneity of $\delta F/F = 1\%$. The line style corresponds to the applied acceleration protocols $a_0(t) \dots a_2(t)$ shown in Fig. 2. The acceleration is limited to $10g = 98.1\text{ m/s}^2$, and Δt adjusted accordingly to achieve the given splitting (thin gray lines). The gray band separates two regimes where either only few phonon modes or essentially all of them contribute (see SI, Sec. S3 for details); it depends on the transverse speed of sound (here: $c = 5.8\text{ km/s}$ for silicon). The band around the dotted yellow line (silicon) represents the effect of the speed of sound from steel (left edge: 3.2 km/s) to diamond (right edge: 12.8 km/s , Ref. [47]).

III. DISCUSSION

From Fig. 4 several facts become evident. For hot objects, BBR decoherence dominates, but this limit is not very relevant as only small spatial splittings are allowed (e.g., 10^{-11} m for an object size of 1 cm). For cold objects, the situation is almost completely reversed. While BBR allows for significant spatial superpositions of large objects, phonons do not. For example, if we cool to a

temperature of 1 K , objects the size of 1 m cannot be put in any spatial superposition. The same applies to objects $10 - 100\text{ m}$ in size (e.g., a car, or a spaceship), even if we cool to much lower temperatures. The results also show that the more adiabatic the force profiles are, the weaker the phonon-induced decoherence is.

It seems there are two ways in which this fundamental limit could be overcome. First, the applied force may be made more homogeneous. This requires that not only the produced potential gradient is highly constant, but also that the material is very pure and homogeneous, or in other words, has near-perfect translational invariance. An example for a homogeneous force is gravity, as long as the particle size is small enough to neglect tidal forces (i.e., assuming the acceleration g to be constant, see SI, Sec. S2). Second, that a high-level of adiabaticity will be reached, although this requires long durations (longer rise time and/or smaller maximal acceleration) meaning that BBR decoherence will kick in. Both of these paths would require extreme precision and novel techniques.

While other hypothesised internal decoherence mechanisms require extensions to standard quantum theory (e.g., the Diosi-Penrose gravitationally induced collapse model, or the GRW / CSL collapse models [48]), the mechanism presented here does not require any such extension.

IV. CONCLUSION

To conclude, we have described a universal and fundamental limit on spatial coherence, which originates from the environment internal to an object and therefore cannot be suppressed by isolation from the external environment. This new decoherence channel puts stringent constraints on any hope for future spatial superpositions of large objects.

Supplementary information See the Appendix for details of the calculations and further plots.

Declarations Both authors contributed equally.

Acknowledgments This work is funded in part by the Israeli Science Foundation Grant Nos. 856/18, 1314/19, 3515/20, 3470/21. This research was supported in part by the National Science Foundation under Grant No. PHY-1748958, and C.H. thanks the KITP (University of California at Santa Barbara) for hospitality during the program “Quantum and Thermal Electrodynamic Fluctuations in the Presence of Matter: Progress and Challenges”.

SUPPLEMENTARY INFORMATION

S1. Mechanistic model

We consider a lattice with interatomic forces in the harmonic approximation, leading to the equation of mo-

tion

$$m_i \ddot{x}_i + \sum_j K_{ij} x_j = F_i. \quad (1)$$

Here, the atom labelled i is displaced by x_i from its equilibrium position (x_{0i}), and the matrix elements K_{ij} specify the interatomic spring constants. The external force is $F_i = -\alpha_i U'(x_{0i})$, where U is the externally applied potential, and α_i is the coupling strength of the i 'th atom to this potential. We first construct the normal modes of the lattice, using the eigenvectors $u_i^k = u^k(x_{0i})$ of the dynamical matrix:

$$\sum_j \frac{K_{ij}}{\sqrt{m_i m_j}} u_j^k = \omega_k^2 u_i^k \quad (2)$$

where ω_k is the normal mode (phonon) frequency. The centre-of-mass (c.m.) mode corresponds to a zero-frequency eigenvector $u_i^0 \propto \sqrt{m_i}$ which exists because of global translation invariance of the potential energy, i.e., $\sum_j K_{ij} = 0$. All normal modes can be chosen real and orthogonal, and be normalised according to $\sum_i u_i^k u_i^l = \delta_{kl}$. Expanding the displacements into normal modes, $x_i(t) = \sum_k q_k(t) u_i^k / \sqrt{m_i}$ with mass-weighted mode amplitudes $q_k(t)$ (unit: length times root of mass), the energy of the lattice takes the diagonal form

$$H = \sum_i \frac{m_i}{2} \dot{x}_i^2 + \sum_{ij} \frac{K_{ij}}{2} x_i x_j = \frac{1}{2} \sum_k (\dot{q}_k^2 + \omega_k^2 q_k^2). \quad (3)$$

Project the equation of motion (1) onto the normal mode k to find

$$\ddot{q}_k + \omega_k^2 q_k = f_k(t) := \sum_i \frac{u_i^k F_i}{\sqrt{m_i}}. \quad (4)$$

where $f_k(t)$ is the force acting on phonon mode k . This is the equation of a driven oscillator with the solution (depicted in Fig. 3)

$$q_k(t) = q_k(0) \cos \omega_k t + \dot{q}_k(0) \frac{\sin \omega_k t}{\omega_k} + \int_0^t dt' \frac{\sin \omega_k(t-t')}{\omega_k} f_k(t'). \quad (5)$$

In the phase-space spanned by the canonical coordinates q_k and \dot{q}_k (we recall that the transformation to the normal mode basis is symplectic [49]), Eq. (5) combines a free rotation by the angle $\omega_k t$ and a translation of the mode amplitude. The integral term gives the displacement $\frac{1}{2} \Delta q_k(t)$ of the in-phase component q_k , while the in-quadrature component \dot{q}_k is shifted by

$$\frac{1}{2} \Delta \dot{q}_k(t) = \int_0^t dt' \cos[\omega_k(t-t')] f_k(t'), \quad (6)$$

its time derivative. Due to the factors $\frac{1}{2}$, a quantity like $\Delta q_k(t)$ is the (mass-weighted) differential displacement of the phonon amplitude between the two arms of the interferometer.

S2. Quantum orthogonality

In quantum theory, the transformation (5) becomes a combination of a rotation (free evolution at ω_k) and a displacement operator \hat{D}_k [50], written here with canonically conjugate operators \hat{q}_k and \hat{q}_k ,

$$\hat{D}_k(t) = \exp \frac{i}{2\hbar} [\Delta \dot{q}_k(t) \hat{q}_k - \Delta q_k(t) \hat{q}_k]. \quad (7)$$

If we start in the Schrödinger picture from a stationary state $|\psi_k(0)\rangle$ for the normal mode k , then the applied force generates the state

$$|\psi_k(t)\rangle = \hat{D}_k(t) |\psi_k(0)\rangle, \quad (8)$$

up to a phase factor independent of $\hat{D}_k(t)$. This scheme provides a spatially separated wave packet if, for example, the sign of the force is controlled by a quantum variable like a spin. In Refs. [18, 36], experiments were done with atoms carrying an unpaired electron and a magnetic gradient force proportional to some projection of the spin magnetic moment (Stern-Gerlach effect, [8, 35, 51]). At the end of the splitting scheme, after spatial recombination and just before detection, the object is in the superposition quantum state

$$|\psi(\Delta t)\rangle = \frac{1}{\sqrt{2}} (|\psi^+(\Delta t)\rangle + e^{i\phi} |\psi^-(\Delta t)\rangle), \quad (9)$$

where the superscript flips the sign of the displacement variables in Eq. (7)

$$|\psi^\pm(\Delta t)\rangle = \bigotimes_k \hat{D}_k^\pm(\Delta t) |\psi(0)\rangle, \quad (10)$$

and the (tensor) product is taken over all normal modes of the particle. The state (9) gives rise to interference fringes, as the phase difference ϕ is scanned. Their normalised contrast turns out as the mode product

$$\begin{aligned} C &= |\langle \psi^+(\Delta t) | \psi^-(\Delta t) \rangle| \\ &= \prod_k |\text{Tr} [\hat{D}_k^2(\Delta t) |\psi_k(0)\rangle \langle \psi_k(0)|]| \\ &= \prod_k |\text{Tr} [\hat{D}_k^2(\Delta t) \rho_k(0)]|. \end{aligned} \quad (11)$$

This formula illustrates that the non-closing of the loop in any normal mode reduces the interference contrast. We made here the assumption that the initial state $|\psi(0)\rangle$ factorises into normal modes $|\psi_k(0)\rangle$, this is valid in the harmonic approximation. Note also that the second line of Eq. (11) generalises the contrast to an initial state $\rho_k(0)$ that is mixed, e.g. the thermal equilibrium state for each phonon mode.

The evaluation of the traces in Eq. (11) is simple using the Wigner representation $W_k(q, \dot{q})$ of the density operator where it leads to the so-called Glauber formula. For

a harmonic mode, the equilibrium Wigner function is the double Gaussian

$$W_k(q, \dot{q}) = N \exp \left(-\frac{q^2}{2\sigma_u^2} - \frac{\dot{q}^2}{2\sigma_v^2} \right), \quad (12)$$

and one gets

$$\text{Tr} [\hat{D}_k^2(\Delta t) \rho_k(0)] = \exp \left[-\frac{1}{2\hbar^2} (\Delta q_k^2 \sigma_v^2 + \Delta \dot{q}_k^2 \sigma_u^2) \right]. \quad (13)$$

From the energy per mode (3), the thermal equilibrium Wigner function contains the variances

$$\sigma_u^2 = \frac{\hbar}{2\omega_k} \coth \frac{1}{2}\beta\omega_k, \quad \sigma_v^2 = \frac{\hbar\omega_k}{2} \coth \frac{1}{2}\beta\omega_k, \quad (14)$$

where $\beta = \hbar/k_B T$ with the internal temperature T (per normal mode). Putting all the above together, we get for the logarithm of the interference contrast the mode sum

$$\log C = - \sum_k \frac{\coth \frac{1}{2}\beta\omega_k}{\hbar\omega_k} \left| \int_0^{\Delta t} dt e^{i\omega_k t} f_k(t) \right|^2, \quad (15)$$

where $f_k(t)$ was defined by Eq. (4).

As a simple check, consider the case that the force acting on the object's i th atom is gravity, $F_i = gm_i$ with a spatially homogeneous acceleration g . This is admittedly not very practical for a controlled splitting, but it is interesting to note that the force projections on the normal modes are

$$f_k = \sum_i g u_i^k \sqrt{m_i} = g \sqrt{M} \delta_{k,0}. \quad (16)$$

Such a force couples *only* to the c.m. mode $k = 0$, a nice illustration of the equivalence principle. The term $k = 0$ in the contrast (15) can be made finite by assuming that the c.m. coordinate is initially distributed with a certain width σ_x . This fixes the variances in Eq. (14) to $\sigma_u^2 = \sigma_x^2 M$, where M is the object's total mass, and $\sigma_v^2 = k_B T$ with its kinetic temperature T . The contrast reduction can be expressed in terms of the *final differential displacements* Δx_f , Δp_f in c.m. position and momentum

$$\log C_{\text{cm}} = -\frac{\Delta x_f^2}{2\lambda_T^2} - \frac{1}{2} \left(\frac{\Delta p_f \sigma_x}{\hbar} \right)^2, \quad (17)$$

with the thermal de Broglie wavelength λ_T of the *entire* object, $\lambda_T^2 = \hbar\beta/M$. This formula illustrates the accuracy that is required in “closing the loop” in phase-space. We recall that $\frac{1}{2}\Delta x_f$ is the displacement in one arm of the interferometer from its initial position; for a wavepacket split with symmetrically opposite forces, Δx_f measures its spatial non-perfect overlap at time $t = \Delta t$.

S3. Summing over phonons

We now turn to the contrast reduction due to the excitation of phonons. For a macroscopic object, the force

F_i on atom i will in general not be proportional to m_i , and it is unavoidable to excite phonons. We elaborate in the following a simple model based on impurity atoms that are randomly distributed across the object. We estimate the contrast, averaged over the impurity distribution, with the Jensen inequality to be $\overline{e^{-\xi}} \geq e^{-\bar{\xi}}$ and consider a simple, spatially uncorrelated model for the force correlation function

$$\overline{F_i(t)F_j(t')} = \delta_{ij} m_i m_j \frac{\delta F^2}{F^2} a(t) a(t'). \quad (18)$$

The relative amplitude of the force inhomogeneities, $\delta F^2/F^2$, turns out to be the key parameter, and $a(t)$ is the acceleration per “average atom” with reference mass m_1 . Any finite-range spatial correlation in the force F_i would lower its power spectrum at short scales, reducing the excitation of phonons with the corresponding wavelengths. The model (18) is therefore expected to provide an upper limit for the phonon-related orthogonality. We also focus on a c.m. dynamics with a perfectly closed loop so that Δx_f and Δp_f in Eq. (17) vanish. We find for the resulting average contrast

$$\log \overline{C} \geq -\frac{\delta F^2}{F^2} m_1 \sum_{k \neq 0} \frac{\coth \frac{1}{2}\beta\omega_k}{\hbar\omega_k} |\tilde{a}(\omega_k)|^2, \quad (19)$$

where $\tilde{a}(\omega)$ is the Fourier transform of $a(t)$, evaluated over the finite experiment time $t = 0 \dots \Delta t$.

We distinguish in the following between two limits: only a few phonon modes are relevant if during the time Δt , sound (with speed c) has made many round trips across its size L , i.e., $c\Delta t/L \gg 1$. The opposite limit where many modes contribute corresponds to a “large” object: sound waves originating from the object's surface, for example, have not yet reached the other end when the recombination occurs in the interference experiment. The “fundamental tone” $\omega_1 \sim \pi c/L$ of the phonon spectrum is a wave that fits within the boundaries of the object, it is in the GHz range for typical condensed-matter values of c and objects smaller than a micron (see Fig. 1). The upper limit of the acoustic mode spectrum is of the order of the Debye frequency (at the Brillouin zone boundary of the phonon band structure), typically a few THz. The temperature dependence embodied in the parameter β in Eq. (19) is such that $\beta \approx 1.9 \text{ ps}$ (25 fs) at $T = 4 \text{ K}$ (300 K), respectively. In most cases, the classical approximation $\coth \frac{1}{2}\beta\omega_k \approx 2k_B T/(\hbar\omega_k)$ is therefore applicable.

a. Few modes. The few-mode regime corresponds to the parameters above the slanted gray band in Fig. 4. Due to the finite interaction time, the Fourier transform $\tilde{a}(\omega)$ is band-limited to $\omega\Delta t \lesssim 1$. For a small object, the fundamental tone ω_1 is beyond this limit, and the sum (19) over eigenfrequencies converges rapidly with only a few terms contributing significantly. In the acoustic spectrum of a sphere, it is therefore sufficient to keep only the two lowest acoustic eigenfrequencies (torsional

and spheroidal d-waves, see Fig. 1) when evaluating the contrast (19).

It is convenient to exhibit in the acceleration profile the maximum spatial splitting Δx between the wave packets, according to

$$\tilde{a}(\omega_1) = \frac{\Delta x}{\Delta t} A(\omega_1 \Delta t), \quad (20)$$

where $A(\omega_1 \Delta t)$ is a dimensionless function with a maximum of order unity. With this, Eq. (19) becomes

$$\log \bar{C} \gtrsim -10 \frac{\delta F^2}{F^2} \frac{\Delta x^2}{\lambda_1^2} \frac{|A(\omega_1 \Delta t)|^2}{(\omega_1 \Delta t)^2}. \quad (21)$$

Here, λ_1 is the thermal de Broglie wavelength for a *single* representative atom (mass m_1 , kinetic temperature T). In the following, we consider three generic protocols for the applied splitting force, sketched in Fig. 2 and with Fourier transforms

$$A_0(\omega \Delta t) = \frac{16}{\omega \Delta t} [\sin(\omega \Delta t/2) - 2 \sin(\omega \Delta t/4)] \quad (22)$$

$$A_1(\omega \Delta t) = -\frac{96}{(\omega \Delta t/2)^2} \left[\cos(\omega \Delta t/2) \left(1 - \frac{60}{(\omega \Delta t)^2} \right) - \frac{\sin(\omega \Delta t/2)}{\omega \Delta t/2} \left(6 - \frac{60}{(\omega \Delta t)^2} \right) \right] \quad (23)$$

$$A_2(\omega \Delta t) = -3\pi^4 \frac{\sin(\omega \Delta t/2)}{(\omega \Delta t/2)^3} \times \left(1 - \frac{(2\pi)^2}{(\omega \Delta t)^2} \right)^{-1} \left(1 - \frac{(4\pi)^2}{(\omega \Delta t)^2} \right)^{-1}. \quad (24)$$

They have in common a spatial splitting Δx at mid-time $\Delta t/2$, but differ in the degree of discontinuity as the force is switched on and off. A_0 , e.g., corresponds to a rectangular profile, namely, less adiabatic. This has tremendous implications for the contrast reduction, as can be seen in Fig. 4. We plot in that Figure those parameter combinations that lead to a contrast $\bar{C} = 1/e$. To simplify the summation over the mode spectrum, we replace the Fourier transforms $|A_n(\omega \Delta t)|^2$ for large enough frequencies, i.e., $\omega \Delta t \gtrsim \pi$, by power laws whose exponent $-2(n+1)$, $n = 0, 1, 2$, can be read off from Eqs. (24). We have checked that this procedure is in good agreement with a summation over the lowest approx. 200 eigenfrequencies.

b. Many modes. This limiting case is defined by the inequality $\omega_1 \Delta t \ll 1$ or a size $L \gg c \Delta t$. Sound waves do not cross the entire object during the interaction time so that the details of the phonon spectrum become irrelevant. In Eq. (19), the sum over modes may then be evaluated by integrating. Keeping three acoustic branches with an average speed of sound \bar{c} and adopting again the classical approximation, we find from Eq. (19)

$$\log \bar{C} \gtrsim -\frac{\delta F^2}{F^2} \frac{3k_B T m_1 V}{\hbar^2 \pi \bar{c}^3} \int_0^\infty \frac{d\omega}{\pi} |\tilde{a}(\omega_k)|^2, \quad (25)$$

Note that this expression only depends on the object volume V and no longer on its aspect ratio. We checked its accuracy by summing over the eigenfrequencies of a large sphere. Inserting the scaling (20) and performing the integration, we get

$$\log \bar{C} \gtrsim -\frac{3\alpha_n}{\pi} \frac{\delta F^2}{F^2} \frac{V}{(\bar{c} \Delta t)^3} \frac{\Delta x^2}{\lambda_1^2} \quad (26)$$

with numerical coefficients $\alpha_n = 64, 58.51, 97.41$ ($n = 0, 1, 2$). In Fig. 4, the parameter sets defined by $\bar{C} = 1/e$ using Eqs. (21, 26) cross in the gray band where $\omega_1 \Delta t \sim 1$ holds. We recall that the different scaling laws in the few-mode limit arise due to the way high frequencies are suppressed in the spectrum of the applied splitting pulse.

S4. Decoherence from blackbody photons

Here we discuss decoherence due to blackbody radiation (BBR). We take into account the momentum exchange due to absorption and emission of photons and characterise it by the diffusion coefficient D_p of Schlosshauer [46] and Romero-Isart [22]. The limiting cases of a small Rayleigh scatterer (radius smaller than the Wien wavelength) and of large object (absorption given by the geometrical cross section) are interpolated with a Padé approximation. The optical constants for the infrared absorption are taken from Ref. [22]. The contrast reduction for the case of a time-dependent applied force is computed from the integral

$$\log C_{\text{BBR}} = - \int_0^{\Delta t} dt \frac{D_p}{\hbar^2} \Delta x^2(t), \quad (27)$$

where $\Delta x(t)$ is the time-dependent spatial separation between the two wave packets. Equation (27) provides the washing-out of the interference fringes (“ghost component”) of the Wigner function for a superposition of wavepackets [50], due to momentum diffusion as thermal photons are absorbed or emitted. This is valid as long as Δx remains small compared to the coherence length of the blackbody field, itself of the order of the Wien wavelength [22, 52]. The integral can be evaluated analytically for the applied force protocols of Fig. (2).

S5. Decoherence parameter space for other accelerations

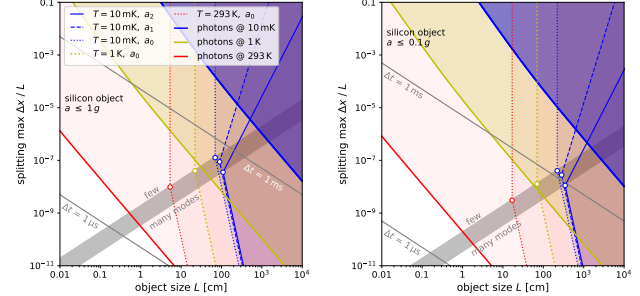


FIG. S1. Same as Fig. 4 of the main text, but for smaller maximum accelerations, limited to 1 g (left) and 0.1 g (right) with terrestrial gravity $g = 9.81\text{ m/s}^2$.

[1] R. S. Aspden, M. J. Padgett, and G. C. Spalding, *Video recording true single-photon double-slit interference*, Am. J. Phys. **84**, 671 (2016).

[2] S. Frabboni *et al.*, *The Young-Feynman two-slits experiment with single electrons: Build-up of the interference pattern and arrival-time distribution using a fast-readout pixel detector*, Ultramicroscopy **116**, 73 (2012).

[3] R. Rosa, *The Merli-Missiroli-Pozzi Two-Slit Electron-Interference Experiment*, Phys. Perspect. **14**, 178 (2012).

[4] H. Rauch and S. A. Werner, *Neutron Interferometry*, 2nd ed. (Oxford University Press, Oxford, 2015).

[5] S. Sala, A. Ariga, A. Ereditato, R. Ferragut, M. Giannetti, M. Leone, C. Pistillo, and P. Scampoli, *First demonstration of antimatter wave interferometry*, Science Adv. **5**, eaav7610 (2019).

[6] A. D. Cronin, J. Schmiedmayer, and D. E. Pritchard, *Optics and interferometry with atoms and molecules*, Rev. Mod. Phys. **81**, 1051 (2009).

[7] S. Abend *et al.*, in *Proceedings of the International School of Physics "Enrico Fermi", Course 197: "Foundations of Quantum Theory"*, edited by E. M. Rasel, W. P. Schleich, and S. Wölck (IOS Press, Amsterdam, 2019), Vol. 119, pp. 345–92.

[8] M. Keil *et al.*, in *Molecular Beams in Physics and Chemistry*, edited by B. Friedrich and H. Schmid-Böcking (Springer, Berlin, 2021), pp. 263–301.

[9] Y. Y. Fein, P. Geyer, P. Zwick, F. Kialka, S. Pedalino, M. Mayor, S. Gerlich, and M. Arndt, *Quantum superposition of molecules beyond 25 kDa*, Nature Phys. **15**, 1242 (2019).

[10] A. Shayeghi, P. Rieser, G. Richter, U. Sezer, J. H. Rodewald, P. Geyer, T. J. Martinez, and M. Arndt, *Matter-wave interference of a native polypeptide*, Nature Commun. **11**, 1447 (2020).

[11] H. Pino, J. Prat-Camps, K. Sinha, B. P. Venkatesh, and O. Romero-Isart, *On-chip quantum interference of a superconducting microsphere*, Quantum Sci. Technol. **3**, 25001 (2018).

[12] C. Wan *et al.*, *Free Nano-Object Ramsey Interferometry for Large Quantum Superpositions*, Phys. Rev. Lett. **117**, 143003 (2016).

[13] S. Bose *et al.*, *Spin entanglement witness for quantum gravity*, Phys. Rev. Lett. **119**, 240401 (2017).

[14] C. Marletto and V. Vedral, *Gravitationally induced entanglement between two massive particles is sufficient evidence of quantum effects in gravity*, Phys. Rev. Lett. **119**, 240402 (2017).

[15] R. Marshman, A. Mazumdar, G. Morley, P. Barker, S. Hoekstra, and S. Bose, *Mesoscopic interference for metric and curvature, and gravitational wave detection*, New J. Phys. **22**, 083012 (2020).

[16] C. Marletto and V. Vedral, *On the testability of the equivalence principle as a gauge principle detecting the gravitational t^3 phase*, Front. Phys. **8**, 176 (2020).

[17] D. Carney, H. Müller, and J. Taylor, *Using an atom interferometer to infer gravitational entanglement generation*, Phys. Rev. X Quantum **2**, 030330 (2021), erratum: Phys. Rev. X Quantum **3**, 010902 (2022).

[18] Y. Margalit *et al.*, *Realization of a complete Stern-Gerlach interferometer: Towards a test of quantum gravity*, Science Adv. **7**, eabg2879 (2021).

[19] F. Kialka, Y. Y. Fein, S. Pedalino, S. Gerlich, and M. Arndt, *A roadmap for universal high-mass matter-wave interferometry*, AVS Quantum Sci. **4**, 020502 (2022).

[20] L. Diósi, *Models for universal reduction of macroscopic quantum fluctuations*, Phys. Rev. A **40**, 1165 (1989).

[21] W. Marshall, C. Simon, R. Penrose, and D. Bouwmeester, *Towards quantum superpositions of a mirror*, Phys. Rev. Lett. **91**, 130401 (2003).

[22] O. Romero-Isart, *Quantum superposition of massive objects and collapse models*, Phys. Rev. A **84**, 052121 (2011).

[23] R. Howl, R. Penrose, and I. Fuentes, *Exploring the unification of quantum theory and general relativity with a Bose-Einstein condensate*, New J. Phys. **21**, 043047 (2019).

[24] I. Fuentes and R. Penrose, in *Collapse of the Wave Function: Models, Ontology, Origin, and Implications*, edited by S. Gao (Cambridge Univ. Press, Cambridge, 2018), pp. 187–206.

[25] M. Rademacher, J. Millen, and Y. L. Li, *Quantum sensing with nanoparticles for gravimetry: when bigger is better*, *Adv. Opt. Techn.* **9**, 227 (2020).

[26] D. E. Chang, C. A. Regal, S. B. Papp, D. J. Wilson, J. Ye, O. Painter, H. J. Kimble, and P. Zoller, *Cavity optomechanics using an optically levitated nanosphere*, *Proc. Natl. Acad. Sci. (U.S.A.)* **107**, 1005 (2009).

[27] A. Albrecht, A. Retzker, and M. B. Plenio, *Testing quantum gravity by nanodiamond interferometry with nitrogen-vacancy centers*, *Phys. Rev. A* **90**, 033834 (2014).

[28] J. Bateman, S. Nimmrichter, K. Hornberger, and H. Ulbricht, *Near-field interferometry of a free-falling nanoparticle from a point-like source*, *Nature Commun.* **5**, 4788 (2014).

[29] T. W. van de Kamp, R. J. Marshman, S. Bose, and A. Mazumdar, *Quantum gravity witness via entanglement of masses: Casimir screening*, *Phys. Rev. A* **102**, 062807 (2020).

[30] M. Schut, J. Tilly, R. J. Marshman, S. Bose, and A. Mazumdar, *Improving resilience of quantum-gravity-induced entanglement of masses to decoherence using three superpositions*, *Phys. Rev. A* **105**, 032411 (2022).

[31] S. Kotler *et al.*, *Direct observation of deterministic macroscopic entanglement*, *Science* **372**, 622 (2021).

[32] L. M. de Lépinay, C. F. Ockeloen-Korppi, M. J. Woolley, and M. A. Sillanpää, *Quantum mechanics-free subsystem with mechanical oscillators*, *Science* **372**, 625 (2021).

[33] B. Schrinski, Y. Yang, U. von Lüpke, M. Bild, Y. Chu, K. Hornberger, S. Nimmrichter, and M. Fadel, *Macroscopic Quantum Test with Bulk Acoustic Wave Resonators*, *Phys. Rev. Lett.* **130**, 133604 (2023).

[34] M. Bild, M. Fadel, Y. Yang, U. von Lüpke, P. Martin, A. Bruno, and Y. Chu, *Schrödinger cat states of a 16-microgram mechanical oscillator*, *Science* **380**, 274 (2023).

[35] W. Gerlach and O. Stern, *Der experimentelle Nachweis der Richtungsquantelung im Magnetfeld*, *Z. Phys.* **9**, 349 (1922).

[36] O. Amit *et al.*, *T^3 Stern-Gerlach Matter-Wave Interferometer*, *Phys. Rev. Lett.* **123**, 083601 (2019).

[37] E. Joos and H. D. Zeh, *The emergence of classical properties through interaction with the environment*, *Z. Phys. B: Condensed Matter* **59**, 223 (1985).

[38] W. H. Zurek, *Decoherence and the transition from quantum to classical*, *Physics Today* **44**, 36 (1991).

[39] B.-G. Englert, J. Schwinger, and M. O. Scully, *Is spin coherence like Humpty-Dumpty? I. Simplified treatment*, *Found. Phys.* **18**, 1045 (1988).

[40] J. Schwinger, M. O. Scully, and B.-G. Englert, *Is spin coherence like Humpty-Dumpty? II. General theory*, *Z. Phys. D* **10**, 135 (1988).

[41] M. Scully, B.-G. Englert, and J. Schwinger, *Spin coherence and Humpty-Dumpty. III. the effects of observation*, *Phys. Rev. A* **40**, 1775 (1989).

[42] C. Henkel and R. Folman, *Internal decoherence in nano-object interferometry due to phonons*, *AVS Quantum Sci.* **4**, 025602 (2022).

[43] O. Romero-Isart, *Coherent inflation for large quantum superpositions of levitated microspheres*, *New J. Phys.* **19**, 123029 (2017).

[44] H. Lamb, *On the Vibrations of an Elastic Sphere*, *Proc. London Math. Soc.* **s1-13**, 189 (1882).

[45] C. Gonzalez-Ballester, D. Hümmer, J. Gieseler, and O. Romero-Isart, *Theory of quantum acoustomagnetics and acoustomechanics with a micromagnet*, *Phys. Rev. B* **101**, 125404 (2020).

[46] M. Schlosshauer, *Decoherence and the Quantum-to-Classical Transition* (Springer, Berlin Heidelberg, 2007).

[47] S.-F. Wang, Y.-F. Hsu, J.-C. Pu, J. C. Sung, and L. Hwa, *Determination of acoustic wave velocities and elastic properties for diamond and other hard materials*, *Mater. Chemi. Phys.* **85**, 432 (2004).

[48] G. Gasbarri, A. Belenchia, M. Carlesso, S. Donadi, A. Bassi, R. Kaltenbaek, M. Paternostro, and H. Ulbricht, *Testing the foundation of quantum physics in space via Interferometric and non-interferometric experiments with mesoscopic nanoparticles*, *Commun. Phys.* **4**, 155 (2021).

[49] H. Goldstein, J. L. Safko, and C. P. Poole Jr., *Classical Mechanics*, 3rd ed. (Pearson, Harlow, 2014).

[50] W. Vogel, D.-G. Welsch, and S. Wallentowitz, *Quantum Optics – An Introduction* (Wiley-VCH, Berlin Weinheim, 2001).

[51] R. J. Marshman, A. Mazumdar, R. Folman, and S. Bose, *Constructing nano-object quantum superpositions with a Stern-Gerlach interferometer*, *Phys. Rev. Res.* **4**, 023087 (2022).

[52] C.-C. Cheng and M. G. Raymer, *Long-range saturation of spatial decoherence in wave-field transport in random multiple-scattering media*, *Phys. Rev. Lett.* **82**, 4807 (1999).